

General Disclaimer

One or more of the Following Statements may affect this Document

- This document has been reproduced from the best copy furnished by the organizational source. It is being released in the interest of making available as much information as possible.
- This document may contain data, which exceeds the sheet parameters. It was furnished in this condition by the organizational source and is the best copy available.
- This document may contain tone-on-tone or color graphs, charts and/or pictures, which have been reproduced in black and white.
- This document is paginated as submitted by the original source.
- Portions of this document are not fully legible due to the historical nature of some of the material. However, it is the best reproduction available from the original submission.

X-661-77-8

PREPRINT

TMX - 71267

X-RAY SIGNATURES: NEW TIME SCALES AND SPECTRAL FEATURES

(NASA-TM-X-71267) X-RAY SIGNATURES: NEW
TIME SCALES AND SPECTRAL FEATURES (NASA)
43 p HC A03/MF A01

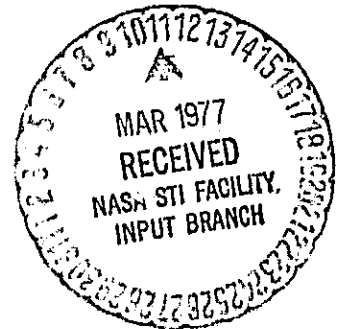
N77-18988

CSSL 03B

Unclas
G3/93 17187

ELIHU BOLDT

JANUARY 1977



— GODDARD SPACE FLIGHT CENTER —
GREENBELT, MARYLAND

X-RAY SIGNATURES: NEW TIME SCALES AND SPECTRAL FEATURES*

Elihu Boldt

Cosmic Radiations Branch
Laboratory for High Energy Astrophysics
NASA/Goddard Space Flight Center
Greenbelt, Maryland 20771

ABSTRACT

The millisecond bursts from Cyg X-1 have been investigated further, and the current status of work on this is presented. The overall chaotic variability for the bulk of the Cyg X-1 emission is compared to that of Sco X-1, showing that the essential character is remarkably similar (i.e. shot noise) although the fundamental time scales involved differ widely, from a fraction of a second (for Cyg X-1) to a fraction of a day (for Sco X-1). A "light curve" constructed via the superposition of millisecond bursts gives evidence for precursor millisecond pulsing at a low duty cycle during the ≈ 1 second interval preceding a burst. An underlying basic period of 9.946 ms implies a Schwarzschild black-hole of more than 8 solar masses.

Recently reported OSO-8 observations of spectral features attributable to iron are reviewed. In particular, line emission is discussed within the context of a model for thermal radiation by a hot evolved gas in systems as different as supernova remnants (e.g. Cas A) and clusters of galaxies (e.g. Coma, Perseus, Virgo). Newly observed spectral structure in the emission from the X-ray pulsar Her X-1 is reported. These features are not simply understood according to standard schemes and might represent some of the new physics to be encountered near a highly magnetized neutron star. In particular, it could be due to iron fluorescence from an Alfvén shell co-rotating with the pulsar, yielding Doppler shifted lines corresponding to speeds up to 0.16c.

* Invited talk, Eighth Texas Symposium on Relativistic Astrophysics, held December 13-17, 1976 at Boston, Massachusetts.

X-RAY SIGNATURES: NEW TIME SCALES AND SPECTRAL FEATURES

Elihu Boldt

Cosmic Radiations Branch
Laboratory for High Energy Astrophysics
NASA/Goddard Space Flight Center
Greenbelt, Maryland 20771

INTRODUCTION

In searching for new X-ray signatures as well as for fine structure in established ones, our group at the Goddard Space Flight Center has made quite extensive observations outside of the usual temporal-spectral regime. During this talk I will be describing a variety of results that have come from this program. This involves a brief review of our observations of Sco X-1, a status report on our study of the rapid variations in Cygnus X-1, including preliminary results on a new effect, and finally, a summary of our recent observations of various spectral features attributable to iron in several objects, ranging from clusters of galaxies to the X-ray binary Her X-1.

Table 1 summarizes our current experiments. For several years we have been carrying out submillisecond timing with rocket-borne experiments. The key features of our current "standard" rocket experiment are 1) the large area (1300 cm^2), 2) the broad spectral response (1.5 - 40 keV) covered with 128 PHA channels, and 3) a pointing system with a stability corresponding to a modulation of much less than 1% for our field of view. At the other extreme, we have an experiment² on Ariel 5 with a particularly small effective area ($\sim 1 \text{ mm}^2$), narrow bandwidth (3-6 keV) and crude temporal resolution ($\sim 10^2 \text{ min}$). However, this images $\sim 80\%$ of the

CURRENT GSFC X-RAY EXPERIMENTS

1. Submillisecond Timing.

Large area detectors on a pointed platform (rocket launched).

2. Long-term Variations (hours - months).

All sky monitor of the brightest sources with a "pin-hole" camera aboard Ariel 5 (Oct '74 -)

3. Spectroscopy (2 - 40 keV).

Proportional chambers aboard OSO-8 (June '75 -)

| | | | |
|---------------|---------------------|-------------------|--------------------|
| PARTICIPANTS: | Robert Becker** | Elihu Boldt * | Stephen Holt |
| | Louis Kaluzienski * | Steven Pravdo | Richard Rothschild |
| | Julia Saba* | Peter Serlemitsos | Richard Shafer* |
| | Barham Smith** | Jean Swank** | |

* University of Maryland (graduate student)

** NAS-NRC Research Associate

sky for any particular orientation of the spacecraft and continuously monitors essentially all sources exceeding about a tenth of the intensity of the Crab Nebula and has been doing this for over two years. Finally, our major current experiment³ is one on OSO-8 devoted mainly to spectroscopy (1.5 - 40 keV) and spectral-temporal correlations down to 20 ms (on special occasions, down to 1.25 ms). Typical net exposures to a given source are on the order of $10^7 \text{ cm}^2 \text{ sec}$, with gross observing times of a few days.

SCORPIUS X-1: A BROADBAND SEARCH

Our search for structure, both temporal and spectral⁴, began several years ago with Sco X-1. It was quite natural that Sco X-1 be the initial object for such a search. With an apparently thermal spectrum with $kT \approx 5 - 6 \text{ keV}$, one would expect that, with near cosmic abundances, the iron line blend at $\sim 6.7 \text{ keV}$ would be most pronounced. In particular we would expect an equivalent continuum width of somewhat more than 1 keV. Since good proportional counters provide an intrinsic resolution of about 1 keV (FWHM) at this energy we expected to see a spectral feature at $\sim 6.7 \text{ keV}$ amounting to at least a 100% increase above the continuum. In a rocket-borne exposure⁴ involving more than 10^5 measured photons from Sco X-1 we obtained a continuum spectrum which did not really fit what one would expect from an optically thin thermal plasma and which did exhibit a 3 σ bulge at about 7 keV that was about 30 times smaller than expected. Since then, Bragg crystal spectral studies by groups at Columbia⁵ and the University of Leicester⁶ have established that there is no appreciable narrow K line emission from iron, with upper limits of a few eV equivalent width. In the meantime, several theoretical studies, starting with that

of Angel⁷, have explained the absence of narrow thermal lines in terms of the severe spectral distortions due to Thomson scattering in a medium with a high column density of electrons. The problem of fitting the Sco X-1 spectrum in detail remains. We have seen this again with our most recent spectral data³² from OSO-8.

With regard to rapid temporal variations, we searched for a suspected pulsar and also possible flickering, as had already been seen in the optical. Using a two-minute continuous exposure involving 0.32 ms temporal resolution¹, we set upper limits of considerably less than 1% on the pulsed fraction of any pulsar variations in the period range 3-360 ms and about 1% for flickering on the scale of several seconds to less than 4% on the scale of tens of milliseconds.

This brings us to our Ariel 5 observation, providing an entirely different view of a source such as Sco X-1. Although the irregular variability of Sco X-1 on long time scales has long been noted, an essentially continuous observation over a few months has enabled us to finally model this variability on time scales of hours or more. The result of this analysis, recently published⁸, is that the bulk of the emission is consistent with a simple two-parameter shot-noise model (i.e. the random overlap of many uncorrelated flare events, where the flare duration and size can be characterized by typical values). The required flare rate is \sim 200 flares per day and the flare duration is about a third of a day. This can be seen qualitatively by looking directly at a sample of the data, shown in Figure 1.

Figure 1 shows the directly inferred 3-6 keV flux from Sco X-1 as a function of time in units of 100 minutes, which is the satellite's orbit

time. The actual number of counts per orbit from Sco X-1 is only ~ 300 . The feature we note is that, for the most part, adjacent bins appear correlated and that this correlation lasts for several bins. An autocorrelation analysis of $\sim 10^3$ orbits yields an e-folding time of about 5 orbits. With such a characteristic duration of about a third of a day and 200 events per day we expect that at any given time there would be about 70 overlapping events. Since the statistical rms deviation on 70 uncorrelated events is about 8, this translates $\sim 10\%$ fluctuations over times longer than a third of a day, and that is the sort of fluctuations we see here. We have also searched one year's data record for the 0.787 day binary period associated with the Sco X-1 optical candidate and find an upper limit⁹ of 1% compared with 25% modulation of the optical amplitude. Although a persistent X-ray modulation at the binary period is absent, we recall that shot-noise is rich in quasi-periodicities¹⁰ and that for events of a third of a day duration the wide range of periods clusters about two-thirds of a day.

CYGNUS X-1 FLUCTUATIONS

Our analysis of the apparently chaotic long-term variations of Sco X-1 was a direct outgrowth of a similar study we did for Cyg X-1 with respect to short-term variations¹¹. Following the original suggestion of Terrell¹⁰ that the rich quasi-periodic variations on the order of 1 s⁻¹ discovered with UHURU were manifestations of shot-noise, we have made rather detailed further investigations of this. Our most recent analysis involves a three minute exposure with our standard rocket payload¹². We estimate the shot pulse rate by examining the variance in the counts

obtained for different sample times; this is shown in Figure 2. Here we plot the observed variance per sample time versus the sample time. For Poisson fluctuations due only to the number of counts, we would expect this to be a constant equal to the mean counting rate, and we have verified this sort of behavior¹¹ on these time scales for Cyg X-3. For times short compared with the characteristic shot-pulse duration, we expect this measure to go linearly, as observed here for times less than 1 second. In general, for the limit that we look at times much longer than any of the coherence times for fluctuations this measure should approach a constant. Conversely, the observed flattening (see Figure 2) of the curve proves that these characteristic rapid fluctuation times are bounded within a scale of about 1 second; this means that Cyg X-1 does not exhibit appreciable fluctuations on time scales from about 1 second up to at least 1 minute. The asymptotic value of the variance ($\text{var}(N)$) per sample time (ΔT) exceeds the average count rate ($\bar{N}/\Delta T$) as follows:

$$\frac{\text{var}(N)}{\Delta T} = (\bar{N}/\Delta T) [1 + f (\bar{m} + \text{var}(m)/\bar{m} - 1)] \quad (1)$$

where f is the fraction of the count rate associated with fluctuations arising from uncorrelated events at the source and m is the observed count per event. For simple shot-noise, $\text{var}(m) = \bar{m}$. In this particular exposure to Cyg X-1 in the low state such a model yields $\bar{m} \approx 130$ counts (i.e., $f \lesssim 1$) which, for the mean total counting rate, yields a shot pulse rate $\approx 8 \text{ s}^{-1}$. This is comparable to the result recently obtained by Weisskopf¹³ and his colleagues in their reanalysis of UHURU data for Cyg X-1 in the low state. Their autocorrelation time of about a half-second is comparable to what we obtain¹², which varies somewhat from one ten-second

interval to another with values in the range 0.3 - 0.7 s. Rothschild¹² has performed Monte Carlo simulations of our count rate profile using a single shot-pulse shape and found that the basic character of the bulk of the variations was adequately replicated. However, the occasional pronounced enhancements lasting a fraction of a second (similar to those discussed by Gursky¹⁵) seen in all our observations of Cyg X-1 are not accounted for in this way. This could be evidence for a more complicated shot-noise process with varying pulse amplitudes.

For the most part, the fluctuations in Cyg X-1 and Sco X-1 are remarkably similar in that the bulk of such emission can be attributed to incoherent events. For Cyg X-1, this amounts to contributions from ≈ 4 randomly overlapping events at any one time. For Sco X-1, ≈ 70 events are involved at any one time. The appropriate time scale for Cyg X-1 is a fraction of a second; for Sco X-1 it is a fraction of a day. Perhaps these are the characteristic time scales for turbulence in the accretion disks surrounding these two different compact non-pulsars.

CYG X-1 MILLISECOND BURSTS

I want to say here that our program of rocket experiments devoted to Cyg X-1 in 1973, 1974 and 1976 was initiated as a direct result of discussions that took place at the Sixth Texas Symposium on Relativistic Astrophysics held in New York City in 1972. The objective was to observe and study extremely rapid bursts from a presumed black-hole. As most of you know, millisecond bursts were discovered during our first such flight three years ago and confirmed on our second one. The detailed results from our second flight are soon to be published¹², and I would

like to give a brief status report on some of the new things we think we know about these bursts.

We have now accumulated 13 clearly distinct millisecond bursts in 230 seconds of exposure. On the second flight our basic sample time was 160 μ s, half that we used on the first flight. Five bursts were seen on this second flight, four of which appeared to belong to the same class as far as intensity and spectral content (the spectrum was also consistent with that of the overall emission). To obtain a best picture of the average burst temporal profile we superposed these 4 bursts. The phasing was established by locating the centroid of the count for each burst and aligning them along their centroids. The counts were interpolated accordingly. The result of this superposition is shown in Figure 3. In effect, this is what a portion of the light curve looks like for Cyg X-1. The millisecond duration and absence of significant substructure is the result here. These bursts were located in the first instance using bin widths equal to 1.28 ms, as in our first flight¹⁶. We also searched for bursts in the same manner using bins ranging in width from 160 μ s to 5.12 ms with no additional statistically significant events that had not already been isolated using 1.28 ms bins.

Although the basic scaler time was 160 μ sec., we also had some finer temporal information. For each such 160 μ sec bin, the time interval between the second and first event accumulated was classified as either 1) between 2 - 5 μ s, 2) between 5 and 50 μ s, or 3) greater than 50 μ s. Since the average count per 160 μ sec bin is only about 1.3 during a typical burst, we thought this could give us a good handle on possible structure

on the microsecond scale such as might be expected for an extreme Kerr black hole. Except for the anomalous burst already noted, the distribution of counts was entirely consistent with that expected from the average count rate during each of the bursts. For the anomalous event there was an indication of excessive bunching that was statistically significant for times less than 5 μ s. This event was not only more intense (by a factor of ~ 2) than a typical burst, but also exhibited a harder spectrum.

What can we do to get a more complete "light curve" for the millisecond pulses from Cyg X-1? For one thing, we already know from the shot noise analysis that the longest coherence time in the Cyg X-1 emission is just a fraction of a second. In that sense, a complete "light curve" for the millisecond pulse behavior would be achieved by extending this superposed profile over a time comparable to a second or so instead of the mere 3.5 ms exhibited in Figure 3. We have in fact done this over ± 1 second for all bursts separated by more than 2 seconds. Since this involves many bursts from the first flight as well, a common temporal unit of 320 μ s equal to the resolution of that flight was used as a standard for this composite profile. Although the average counting rate in this complete light curve is about 20% higher during the 1 second interval preceding the burst centroid than during the 1 second interval following the centroid, there is no other obvious structure.

This is where things stood a few weeks ago when I started preparing this talk. Then I realized that we had neglected to sufficiently investigate a potentially important effect that might be peculiar to a black hole. In searching for usual periodic pulsing one implicitly assumes that not

only the frequency, but also the amplitude and phase of the pulsing remains relatively stationary during the time of measurement. However, consider the inner-most stable Keplerian orbits around a black hole. The rotation frequency of matter in such an orbit is certainly a stable number, but a given disturbance here would have a finite lifetime^{17,18}, from a few orbits up to perhaps a hundred or so. Hence, we can not expect long-term phase stability. From our variance analysis, the upper limit would have to be a fraction of a second.

What about amplitude stability? Unlike a highly magnetized neutron star where the dipole field controls the pulsar emission process, radiation from an accretion disk is evidently dominated by random events arising from turbulence. Hence, we have the intriguing possibility of pulsed emission with phase stability lasting up to a second, but where many or even most of the pulses are absent. Those pulses that do occur of course take place at the proper time. However, given a grid of allowed times for a pulse, the probability that one actually occurs could, in the limit, be entirely random.

To investigate this further, we examined the complete listing of the 6250 individual entries making up the composite light curve for the ten bursts aligned along their centroids. Recall that the resolution is 0.32 ms and that this covers a time interval extending from one second before the centroid to one second afterwards. Based upon the mean count per bin during the one-second interval following the centroid, I concluded that a count of 10 per bin should be exceeded in 1.9 cases, on the average, for the composite two-second interval outside the burst. In fact, 8 cases

were found prior to the burst, and 2 were found afterwards.

By noting the smallest intervals among the 8 cases so tagged during the one-second prior to the composite burst, I was struck by the fact that these times were small integer multiples of close to the same basic unit. This common unit was found to be about 31 resolution elements; this corresponds to about 9.9 ms. By fine tuning to a value of 31.08, I found that 5 out of the 8 cases were aligned to within one resolution element (i.e. .32 ms) of the phase defined by the centroid of the composite burst. Detuning to 31 reduces the number of cases so alligned to 2.

To graphically exhibit this new aspect of the light curve, we used a basic 9.964 ms cycle time (i.e. 31.08 resolution elements) to strobe through the entire two-second profile. The phase was arranged so that cycle #100 places the composite burst centroid just at the center of that cycle. Those cycles including the 8 tagged cases prior to the centroid were superposed and compared to cycle #100. This is shown in Figure 4. The bottom graph in Figure 4 shows the composite burst profile. The three central bins (0.96 ms) appear to be an adequate definition of the burst duration. The top graph in Figure 4 is the superposition of the 8 cycles prior to the burst for which we noted > 10 counts in a 0.32 ms bin. The average level expected for the superposition of 8 cycles selected from among the first 99 cycles is shown as a dashed line. For the particular 8 cycles used here the actual average, excluding the three central bins, is a higher number (38.2 counts) and the variations about that value are consistent with statistical fluctuations. The three bins with the highest count appear at the correct phase. Based on the average for the other

bins in this cycle, the enhancement in these three central bins, taken together, represents a 5.7 sigma fluctuation.

Figure 5 exhibits a comparison of cycle #100 with the superposition of the two cycles afterwards tagged on the basis of > 10 counts in a 0.32 ms bin. In this case, there does not appear to be anything special about the three central bins. Using intervals three bins wide, phased to include the three central bins as one interval, the bottom profile does not correspond to a statistically significant variation.

A superposition of the first (or last) 99 cycles, based upon a 9.964 ms cycle time, fails to show any statistically significant structure. Considering this negative result in conjunction with the positive result for selected cycles (Figure 4) shows that, on the average, the integral intensity of precursors is comparable to the intensity of the main burst.

The time from the first noted precursor of > 10 counts/bin to the centroid of the burst profile is 0.696 s, comparable to the longest shot pulse. The general tendency for millisecond variations to cluster over times on this scale had already been noted by Oda et al.³⁹. A picture that emerges is one involving a disturbance in the accretion disk that is carried around inner Keplerian orbits for a fraction of a second at an essentially constant frequency, sometimes emitting radiation in our direction and sometimes not and then disappears after a particularly large burst. If the burst duration is fixed by the eclipse of the disturbance by a black hole (e.g., by focusing¹⁷) then the ratio of burst duration to period may be estimated, in the case of a Schwarzschild metric, as

$$\frac{\Delta T}{\tau} \lesssim \left(\frac{1.5}{\pi} \right) \left(\frac{R_g}{R} \right) \quad (2)$$

where R is the distance of the disturbance from the black hole, R_g is the Schwarzschild radius ($R_g = 2 GM/c^2$) and the inequality allows for observations at angles away from the plane of the disk. Measured in units of the innermost stable Keplerian orbit ($R_o \cong 3 R_g$), Equation 2 yields the radial distance of the disturbance (R) as

$$\frac{R}{R_o} \lesssim 1.7 \pm 0.3 \quad (3)$$

where we have used $\Delta T = (0.96 \pm 0.16)$ ms as the burst duration (see Figure 3) and $\tau = 9.964$ ms as the period.

While the estimated radial distance (Equation 3) of the disturbances giving rise to millisecond bursts is consistent with the radius of maximum brightness (expected^{19,20} at $1.36R_o$) it is difficult to imagine that the required disturbances almost always occur within a radial band at $R > R_o$ sufficiently narrow to account for the apparently sharp period discussed here. However, if they do we can then estimate the mass of the corresponding Schwarzschild black hole, using the following relation¹⁷:

$$\frac{M}{M_o} = \left(\frac{\tau}{6 \times 10^{-4} \text{ s}} \right) \left(\frac{R}{R_o} \right)^{-3/2} \quad (4)$$

From Equations 3 and 4, we obtain

$$\frac{M}{M_o} \gtrsim 8 \pm 2. \quad (5)$$

It should be noted, however, that the shortest possible stable period is that for the innermost stable orbit, given by²⁰

$$\tau = (4.52 \times 10^{-4} \text{s}) M/M_{\odot}. \quad (6)$$

For the mass estimate given by Equation 5, the corresponding period obtained via Equation 6 is

$$\tau \text{ (minimum)} \approx (4 \pm 1) \times 10^{-3} \text{ seconds}. \quad (7)$$

The scale given by Equation 7 is comparable to the shortest interval (≈ 6 ms) obtained from among the four distinct bursts associated with a very pronounced enhancement (i.e. about a three-fold increase of intensity over a fraction of a second) observed during our first experiment. Taken together, these 4 bursts are possibly associated with the same event. At the innermost stable orbit, the burst duration (via Equation 2) corresponding to a period of about 6 ms would become ≈ 1 ms, comparable to that observed.

A more plausible alternative would allow for multiple disturbances at the inner region of the accretion disk, especially during pronounced enhancements. In such a situation we would account for the rare case of bursts exhibiting an interval shorter than the sharp period of 9.964 ms as arising from multiple disturbances azimuthally clumped around the inner region of the accretion disk. In general, the sharp period would be associated with an isolated disturbance while at the innermost stable orbit, prior to extinction by the black hole. On this basis, we estimate the mass of a Schwarzschild black hole via Equation 6 as $M = 22 M_{\odot}$,

somewhat larger than previous estimates arising from considerations of the binary system^{21,22,23}. Any appreciable spin for the black hole appears to be ruled out since such a case (i.e. Kerr metric) would only increase the value for the mass corresponding to a sharp Keplerian period as large as that indicated here for the inner region of the accretion disk.

As referred to earlier, there was one burst during our second experiment¹² which was clearly in a different class from that associated with all the other 12 distinct bursts we have seen to date. The substantially higher intensity, harder spectrum and temporal substructure for this anomalous one might be indicative of an infalling disturbance while in a marginally stable orbit immediately prior to reaching the event horizon²¹.

SPECTROSCOPY: BRIGHT SOURCES

The spectrum of Cygnus X-1 was remarkably constant during these observations¹² just described. As shown in Figure 6, even if we compare data from the two rocket flights involved, which were separated by a year, we get the same spectrum. For this power law spectrum, the number index is $n \approx 1.5$. The three-minute exposure of the second flight was broken into three separate one-minute spectra. Comparing the four one-minute samples we get from the two flights, we conclude that there are no variations (to within $\delta n = \pm 0.04$) either minute to minute or year to year, at least for the low state of Cyg X-1 represented here (at binary phase 0.17).

As is evident from Figure 6, this is an essentially structureless spectrum, although small deviations from a strict power law are not ruled out. The upper limit (3σ) for narrow K line emission by iron corresponds to an equivalent width of ~ 40 eV, comparable to the level expected^{34,35}

for fluorescence from the optical companion when Cyg X-1 is near inferior conjunction (i.e. not the case here).

Our OSO-8 experiment observed Cyg X-1 during a high state in November of last year, when it again exhibited an essentially structureless but steeper spectrum. In addition to Cyg X-1 and Sco X-1 (discussed earlier), some of the other bright sources observed with our OSO-8 experiment to exhibit spectra devoid of any pronounced features includes Cyg X-2 and the Crab Nebula (e.g. see Figure 8).

THERMAL SOURCES

The objects just discussed are evidently not representative of the typical situation in X-ray astronomy. To illustrate this, Figure 7 shows the spectrum we inferred²⁵ for one of the weakest known galactic sources. This thermal spectrum indicates iron K line emission at a level corresponding to an equivalent width of over 1 keV, the sort of result we originally expected for Sco X-1. However, this source corresponds to only 3 UHURU counts (i.e. $\sim 6 \times 10^3$ times less than the intensity of Sco X-1). If we make a tentative identification with the radio supernova remnant G297.8 - 0.5, then we can classify this source with other young remnants such as Cas A²⁶ and Tycho^{26,27} which also show strong iron K line emission.

We study these apparent line features in thermal spectra by assuming optically thin emission by an isothermal plasma, omitting any line emission expected from iron, fitting the continuum to an optimum temperature and then examining what remains. This is illustrated³² in Figure 8. The residual for Cas A corresponds to a narrow line at 6.7 keV. The connected levels shown here give the expected response to a sharp line of the observed

intensity at 6.7 keV and is determined entirely by the measured resolution function of the detector itself. At a temperature of ~ 50 million degrees (that for the hot component of Cas A) the dominant lines are from helium type ions of iron at energies of 6.70, 6.68 and 6.65 keV, and we call this the "6.7 keV blend". For a temperature of 80 million degrees (such as for the Perseus cluster of galaxies) the hydrogenic ions of iron make a non-negligible contribution at 6.97 keV ("7 keV"). If we take into account the expected redshift ($z = 0.018$) of ~ 120 eV, it just about compensates for the increased mean energy of the feature. The lack of narrow iron K-line emission from the Crab Nebula corresponds to an upper limit (3 σ) for the equivalent width of about 30 eV.

Most of our data on the Perseus, Virgo and Coma clusters are now in hand. Our preliminary analysis of these data indicate that our earlier conclusions²⁸ based upon about 10% of the data in each instance have remained substantially the same. At that stage, a simple isothermal model was adequate, with the possible exception of Virgo. We considered only the 6.7 keV line blend of helium-type iron. We have not as yet considered other models, such as an adiabatic model. Nor have we as yet considered small spectral features such as would arise from iron K β line emissions and an iron emission edge. Effects due to calcium, argon, sulphur and silicon are probably less important, if our temperature estimates for these clusters are at all correct. With these qualifications, Figure 9 summarizes the results obtained from the first 10% of our data. These theoretical curves were calculated²⁹ for an isothermal optically thin plasma at collisional equilibrium. The key parameters involve the abundances

of iron and helium relative to hydrogen. The numbers used were 4×10^{-5} for iron and 8.5% for helium. We consider separately the $K\alpha$ line from helium and hydrogen type ions, and these are given by the solid curves. The dashed curve gives the effective total equivalent width for an experiment which combines these two energies into a single spectral feature. The remarkable thing about this plot is that it shows that the line emission from each of these very different clusters is consistent with the same thermal model. In particular, it means the same abundance of iron fits all three and that this amounts to about half the value assumed, giving a number of $\sim 2 \times 10^{-5}$ relative to hydrogen. This value is not inconsistent with some estimates³⁰ of solar abundance and is a strong indication that the emitting plasma is a highly evolved gas (e.g. it is probably not primordial matter). The fact that these three clusters are so different in richness, morphology and predominance of active galaxies and yet are so unified in their thermal X-ray characteristics indicates to me that this emission is one of the most fundamental manifestations of a cluster and might turn out to be one of the few unambiguous ways of identifying a cluster. On that basis, we have preliminary indications³² of iron K line emission from two more clusters. One of these is the Centaurus Cluster. The other is a cluster candidate⁴⁰, apparently associated with Cygnus A. The temperature and equivalent width for both of these are comparable to those for Perseus. Three key features of the Cygnus A results which are consistent with the cluster interpretation are 1) the absence of absorption, indicating an extended source, 2) the constant intensity relative to early UHURU observations³¹, indicating the probable absence³¹ of major transient contributions, and 3) the best fit line energy of 6.3 keV, consistent with

the anticipated redshift of 6% down from 6.7 keV.

IRON FLUORESCENCE: HER X-1

Finally, I will summarize some spectral line observations in Her X-1 which have been most puzzling. These have been described in detail in a recently completed thesis by S. Pravdo³³. Here are the main features:

- 1) Averaged over binary cycles, the line is centered at 6.5 ± 0.4 keV, but exhibits appreciable intrinsic broadening (FWHM $\approx 2.4 \pm .7$ keV). The equivalent continuum width is ≈ 340 eV.
- 2) When examined for times short compared with 1.7 days (the binary cycle) the character of the line can be very different. For example, at phase 0.2 of one particular binary cycle the line appears with the correct energy, as shown in Figure 10. However, at phase 0.1 of the next binary cycle the line character is quite different, as shown in Figure 11. In this latter case we have two lines, one at ≈ 5.5 keV and another at ≈ 7.4 keV, and there appears to be a deficiency between $\approx 6 - 7$ keV.
- 3) Line energies vary from 5.5 - 8.2 keV. Sometimes there is a single line, sometimes there are two. There is no apparent correlation with binary phase.
- 4) The equivalent width of the line or the composite equivalent width for two lines remains essentially constant with binary phase.
- 5) With respect to pulsar phase, the off-pulse line emission is broad and relatively strong while the line is probably absent for a portion of the peak of pulsed emission. At pulse minimum, it is consistent with a single line, as shown in Figure 12.

What does all this mean? Consider these alternatives:

- 1) Thermal lines are unlikely since the effective temperature of Her X-1 is probably too high. Furthermore, it is difficult if not impossible to account for all the line energies observed.
- 2) Ordinary fluorescence can account for iron K α line emission between 6.4 and 7 keV depending upon the state of ionization, but it can not simply account for energies as low as 5.5 keV or as high as 8.2 keV.
- 3) There are several possible targets for fluorescence, e.g.
 - a) Iron near the surface of the neutron star might account for the low energies by gravitational red-shift, but not the high energies.
 - b) HZ Her should fluoresce³⁵, but the K α line of low ionized iron should always be at ~ 6.6 keV. In addition, the observed line intensity is probably too high.
 - c) Some absorption dips³³ show unit optical depth for iron. If the region of matter responsible for such dips is somehow always present, it could account for the intensity of the observed line emission by fluorescence, provided it subtends an angle close to 2π sterad. The variable energy observed is a complication.

The only fluorescing target I know of which has any chance of accounting for all the main features of this line emission is the Alfvén shell³⁶.

In such a case the various line energies would be accounted for by Doppler shifts. At the equator, the required velocity is $0.16c$. This shifts

a 6.4 keV line to 5.4 keV and 7.5 keV for emission at the equator; the spectral intensity to be observed at 6.4 keV would be relatively small. Line emission at 7 keV could be shifted as high as 8.2 keV. For a period of 1.24s this requires a radius of 9×10^8 cm, which is comparable to that of an Alfvén shell for Her X-1 recently described by McCray and Lamb³⁷. The magnetic dipole required would correspond to a field of close to 10^{13} G near the poles at the surface of the neutron star; the steep high energy spectral cut-off for the X-ray emission from Her X-1 has already been interpreted³⁸ as a measure of a field with this strength.

When viewed near the equatorial plane of a subrelativistically spinning shell, the monochromatic radiation emitted by a spot on this shell will exhibit a finite spectral density ($dN/dh\nu$) which, when averaged over a cycle, is given by

$$\frac{dN}{d(h\nu)} \propto [1 - (\Delta h\nu/h\nu_0)^2 (R\omega\cos\delta/c)^{-2}]^{-1/2} \quad (8)$$

where $(h\nu)_0$ is the emitted photon line energy, R is the radius of the shell, δ is the latitude of the spot(s), ω is the angular velocity, c is the speed of light and $\Delta h\nu$ is the observed energy shift relative to $(h\nu)_0$. The range for $h\nu$ is in general given by the limits

$$(h\nu)_{\pm} = (h\nu)_0 [1 \pm (R\omega\cos\delta/c)] [1 - (R\omega\cos\delta/c)^2]^{-1/2} \quad (9)$$

From Equations 8 and 9 we note that the apparent spectral density corresponding to a fluorescence line emitted from an Alfvén shell co-rotating with a pulsar will in general exhibit a minimum at the unshifted energy and two essentially symmetrical maxima at the opposite extremes of Doppler

shifted energy.

In conclusion, I call attention to some practical criteria for further studies of spectral lines which emerge from our observations. The sources of narrow lines we discussed earlier are well behaved, associated with emission from extended regions (e.g. thermal plasmas in supernova remnants and clusters of galaxies, the fluorescing atmosphere of the optical member of an X-ray binary) and should therefore be amenable to studies with high resolution dispersive spectrometers where small throughput imposes the requirement of long exposures. However, sources such as Her X-1 which exhibit broad and variable line features require spectrometers of relatively high throughput (e.g. non-dispersive) over an extended band that allows for simultaneous measurements of spectral structure and the continuum.

REFERENCES

1. Boldt, E. A., S. S. Holt and P. J. Serlemitsos. 1971. Search For Temporal Structure in X-rays from Scorpius X-1. Ap. J. 164: L9.
2. Holt, S. S. Temporal X-ray Astronomy with A Pinhole Camera. 1976. Astrophys. and Space Sci. 42: 123.
3. Serlemitsos, P. J., R. H. Becker, E. A. Boldt, S. S. Holt, S. H. Pravdo, R. Rothschild and J. H. Swank. 1976. Cosmic X-ray Observations with OSO-8, in X-ray Binaries, Proceedings of a Symposium held at Goddard Space Flight Center, Greenbelt, Md, October 20-22, 1975. eds. Y. Kondo and E. Boldt. NASA SP-389: 67.
4. Holt, S. S., E. A. Boldt and P. J. Serlemitsos. 1968. Search for Line Structure in the X-ray Spectrum of Sco X-1. Ap. J. 154: L137.
5. Kestenbaum, H., J. R. P. Angel, and R. Novick. 1971. X-ray Spectrum of Scorpius X-1 Obtained with a Bragg Crystal Spectrometer. Ap. J. 164: L87.
6. Griffiths, R. E.. 1972. A Further High Resolution Search for Fe XXV Line Emission from Scorpius X-1. Astron. Astrophys. 21: 97.
7. Angel, J.R.P. 1969. X-ray Line Emission from Sco X-1. Nature 224: 160.
8. Holt, S. S., E. A. Boldt, P. J. Serlemitsos and L. J. Kaluzienski. 1976. Long-Term X-ray Studies of Scorpius X-1. II. Evidence for Flare Dominated Intensity Variations. Ap. J. 205: L79.

9. Holt, S. S., E. A. Boldt, P. J. Serlemitsos and L. J. Kaluzienski. 1976. Long-Term X-ray Studies of Scorpius X-1. I. Search for Binary Periodicity. *Ap. J.* 205: L27.
10. Terrell, N. James Jr. . 1972. Shot-Noise Character of Cygnus X-1 Pulsations. *Ap. J.* 174: L35.
11. Boldt, E., S. Holt, R. Rothschild and P. Serlemitsos. 1975. What Is Special About Cygnus X-1? Proceedings of International Conference on X-rays in Space, Univ. of Calgary, Canada, August 14-21, 1974, (ed.: D. Venkatesan): 69.
12. Rothschild, R. E., E. A. Boldt, S. S. Holt and P. J. Serlemitsos. 1977. High Resolution Measurements of the Low State of Cyg X-1. *Ap. J.* (In press).
13. Weisskopf, M. C. 1976. Private communication.
14. Weisskopf, M. C., S. M. Kahn, and P. G. Sutherland. 1975. Short-term Time Variability of Cygnus X-1. *Ap. J.* 199: L147.
15. Gursky, H. 1977. Proceedings of this symposium.
16. Rothschild, R. E., E. A. Boldt, S. S. Holt and P. J. Serlemitsos. 1974. Millisecond Temporal Structure in Cygnus X-1. *Ap. J.* 189: L13.
17. Sunyaev, R. A. 1972. Variability of X-rays From Black Holes with Accretion Disks. *Astron. Zh.* 49: 941 (translated in *Soviet Astronomy-AJ* 16, 941, 1973).
18. Leach, R. W. and R. Ruffini. 1973. On the Masses of X-ray Sources. *Ap.J.* 180: L15.
19. Shakura, N. I. and R. A. Sunyaev. 1973. Black Holes in Binary Systems. Observational Appearance. *Astron. Astrophys.* 24: 337.

20. Novikov, I. D. and K. S. Thorne. 1973. Astrophysics of Black Holes, in "Black Holes". B. deWitt and C. deWitt, Eds. Gordon and Breach, Science Publishers Inc., New York, N.Y.
21. Hutchings, J. B. 1974. On the Light Curves and Masses of the X-ray Sources Cygnus X-1, SMC X-1 and Cen X-3. Ap. J. 193: L61.
22. Avni, Y. and Bahcall, J. N. 1975. Ellipsoidal Light Variations and Masses of X-ray Binaries. Ap. J. 197: 675.
23. Bolton, C. T. 1975. Orbital Elements and an Analysis of Models for HDE226868 = Cygnus X-1. Ap. J. 200: 269.
24. Stoeger, R. 1976. Private communication.
25. Becker, R. H., E. A. Boldt, S. S. Holt, S. H. Pravdo, R. E. Rothschild, P. J. Serlemitsos and J. H. Swank. 1976. X-ray Emission from the Supernova Remnant G287.8-0.5. Ap. J. 209: L65.
26. Pravdo, S. H., R. H. Becker, E. A. Boldt, S. S. Holt, R. E. Rothschild and P. J. Serlemitsos. 1976. Iron Line Emission from a High Temperature Plasma in Cassiopeia A. Ap. J. 206: L41.
27. Davison, P.J.N., J. L. Culhane and R. J. Mitchell. 1976. X-ray Spectra of Cassiopeia A and Tycho's Supernova Observed with Ariel 5. Ap. J. 206: L37.
28. Serlemitsos, P. J., B. W. Smith, E. A. Boldt, S. S. Holt and J. H. Swank. 1977. X-radiation from Clusters of Galaxies: Spectral Evidence for a Hot Evolved Gas. Ap. J. Letters. (In press).
29. Smith, B. Private communication.
30. Walker, A.B.C., Jr., H. R. Rugge, and K. Weiss. 1974. Relative Coronal Abundances Derived From X-ray Observations III. Ap. J. 194: 471.

31. Giacconi, R., S. Murray, H. Gursky, E. Kellogg, E. Schreier, E. Matilsky, D. Koch and H. Tananbaum. 1974. UHURU (3U) Catalog of X-ray Sources. Ap. J. Suppl. 7: 7.
32. Serlemitsos, P. 1976. Private communication.
33. Pravdo, S. 1976. Hercules X-1: Spectral Variability of an X-ray Pulsar in a Stellar Binary System. Ph.D. dissertation, University of Maryland. GSFC Document X-661-76-280.
34. Swank, J. 1976. Private communication.
35. Basko, M. M., R. A. Sunyaev and L. G. Titarchuk. 1974. Reflection and Reprocessing of X-ray Source Radiation by the Atmosphere of the Normal Star in a Binary system. Astron. Astrophys. 31: 249.
36. Basko, M. M. and R. A. Sunyaev. 1976. The Import of the Alfven Surface for the X-ray Pulse Formation in Accreting Pulsars. Preprint (Space Research Institute, Moscow).
37. McCray, R. and F. K. Lamb. 1976. An Opaque Shell Around Her X-1? Ap. J. 204: L115.
38. Boldt, E., S. Holt, R. Rothschild and P. Serlemitsos. 1976. The Her X-1 Spectrum: A Measure of the Field Near the Magnetic Poles of a Neutron Star. Astron. Astrophys. 50: 161.
39. Oda, M., R. Takagishi, M. Matsuoka, S. Miyamoto and Y. Ogwara. 1974. Millisecond X-ray Pulses from Cyg X-1. Publ. Astron. Soc. Japan 26: 303.
40. Brinkman, A. C., J. Heise, A. J. F. den Boggende, J. Grindlay, H. Gursky and D. Parsignault. 1977. X-ray Observations of the Cygnus A with ANS. Ap. J. (In press).

FIGURE CAPTIONS

Figure 1. Sample Sco X-1 single-orbit data from the all-sky monitor aboard Ariel 5. The apparent coherence of most intensity variations over several orbits is typical of the total Sco X-1 record.

Figure 2. Variance per unit bin width versus bin width (seconds) evaluated for counts from Cyg X-1 obtained in GSFC Flight 26.037 (3 October 1974). The dashed line shows the mean count rate of Cyg X-1 during the three-minute exposure.

Figure 3. Centroid-aligned mean burst profile for the 3 October 1974 observation of Cyg X-1. The temporal bins are 160 μ s wide and the data are from four superposed bursts. The dotted line represents the expected burst profile for a 1 ms wide rectangular pulse containing the same number of counts as the four bursts.

Figure 4. A strobe of the first half of the Cyg X-1 "light curve", at a period of 9.946 ms. The "light curve" from which this is constructed is the centroid-aligned profile of ten bursts (see text) over a two-second interval (i.e. ± 1 second relative to the centroid), at a resolution of 0.32 ms.

Bottom graph: Counts per 0.32 ms bin as a function of temporal phase for cycle #100. The initiation of cycles is determined from a period of 9.946 ms, where the absolute phase is chosen such that cycle #100 exhibits the centroid of the composite burst at bin #16.

Top graph: Superposed counts per 0.32 ms bin as a function of temporal phase for those 8 cycles selected from among the first 99 cycles upon the basis of exhibiting a count > 10 for one or more bins. The dashed

line gives the count per bin expected for a superposition of 8 cycles selected at random from among the first 99.

Figure 5. A strobe of the second half of the Cyg X-1 "light curve", at a period of 9.946 ms. The "light curve" is the same as used for Figure 4.

Bottom graph: Superposed counts per 0.32 ms bin as a function of temporal phase for those 2 cycles selected from among the 99 cycles following cycle #100 upon the basis of exhibiting a count > 10 for one or more bins.

Top graph: Counts per 0.32 ms bin as a function of temporal phase for cycle #100. Same as Figure 4 (bottom graph).

Figure 6. Inferred incident spectra of Cyg X-1 observed on two flights separated by a year (#26.037 on 3 Oct. '74 and #13.010 on 4 Oct. '73).

Binary phase was 0.17 for both observations. The solid circles represent the spectrum seen with a xenon filled detector and the open circles represent the spectrum seen with an argon filled detector.

Figure 7. The inferred incident X-ray spectrum for 4U1043-59. The solid curve represents the best-fit thermal continuum to the data (OSO-8 GSFC X-ray experiment).

Figure 8. The residual count rate ($\text{cm}^{-2} \text{s}^{-1}$) observed per channel relative to the count rate expected from a continuum best-fit to the overall spectrum versus pulse-height-analyzer channel number. The continuum fit used for the Crab Nebula was a power-law spectrum while those used for Cas A and the Perseus Cluster were thermal continua. These data

are from the GSFC X-ray experiment aboard OSO-8. The connected levels shown for Cas A give the expected response of the detector to a sharp line of the observed intensity at 6.7 keV.

Figure 9. The equivalent continuum width (eV) for iron K line emission versus temperature (keV). The data points and associated error bars are for the OSO-8 "quick look" observations²⁸ of three clusters of galaxies (Virgo, Perseus and Coma). The curves were calculated²⁹ on the basis of iron $K\alpha$ emission from an isothermal optically thin plasma at collisional equilibrium. Relative to hydrogen, the abundances used were 4×10^{-5} for iron and 8.5% for helium. The dashed curve is the sum of the solid curves (one for the 6.7 keV blend from helium-type ions of iron and the other for the 6.97 keV line from hydrogenic ions of iron).

Figure 10. The inferred³³ incident X-ray spectrum for Her X-1 at a binary phase 0.2.

Figure 11. The inferred³³ incident X-ray spectrum for Her X-1 at a binary phase 0.1, one cycle subsequent to that associated with Figure 10.

Figure 12. The inferred³³ incident X-ray spectrum ($\text{cm}^{-2}\text{s}^{-1}\text{keV}^{-1}$) for Her X-1 during the portion ($\sim 10\%$) of the pulsar light curve exhibiting minimum intensity.

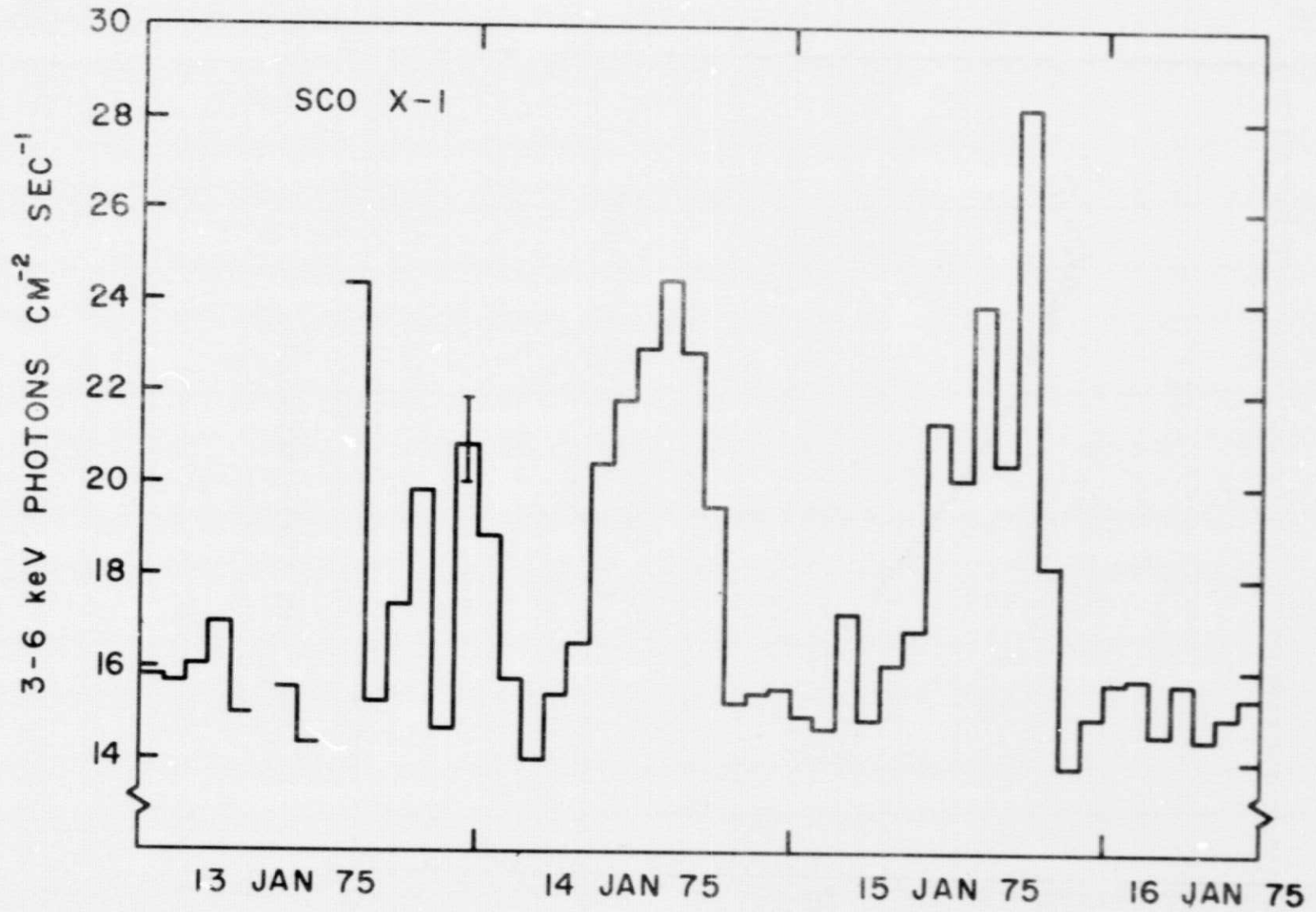


Figure 1

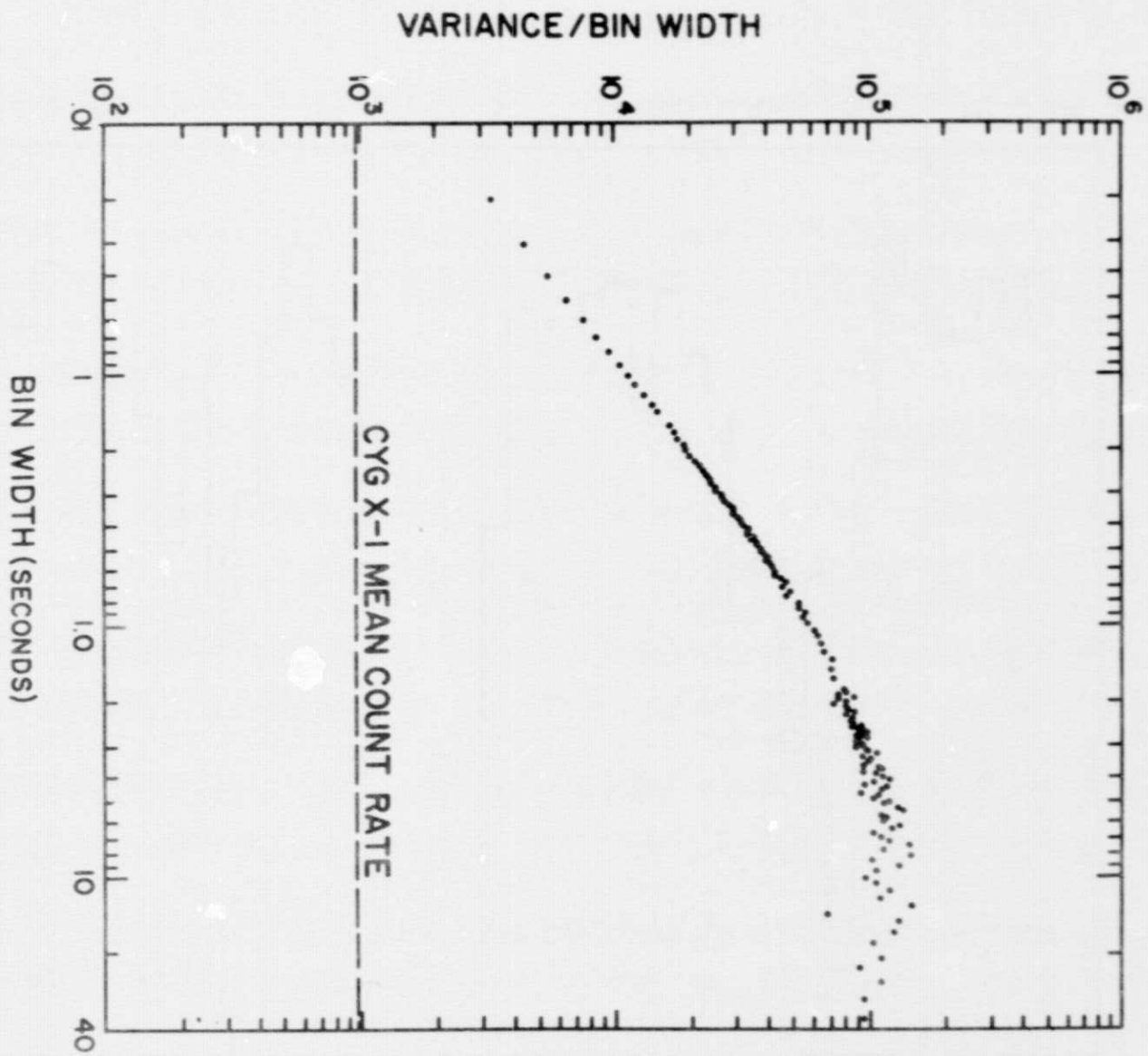


Figure 2

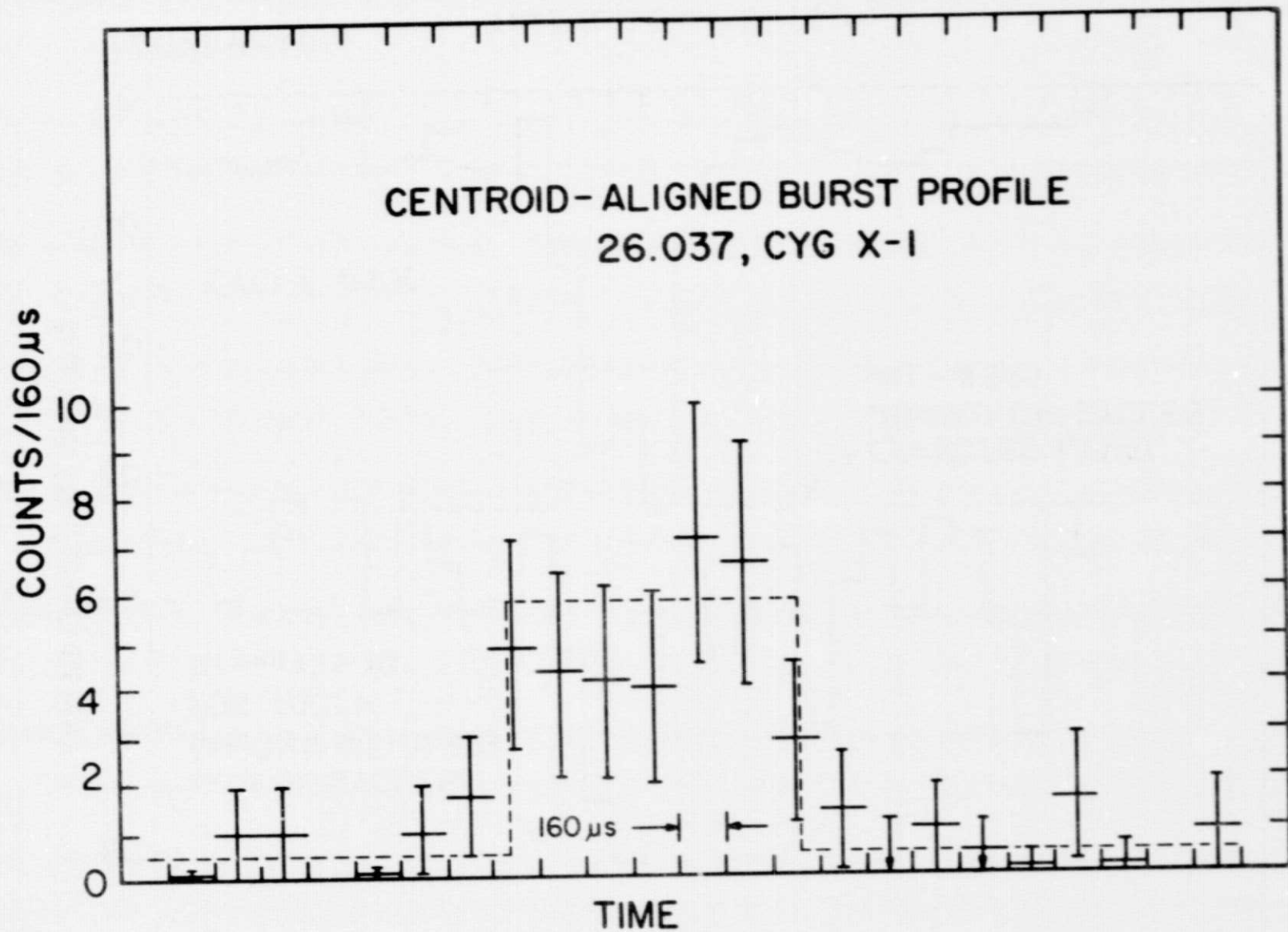


Figure 3

STROBE OF CYG X-1 "LIGHT CURVE" AT 9.946ms PERIOD

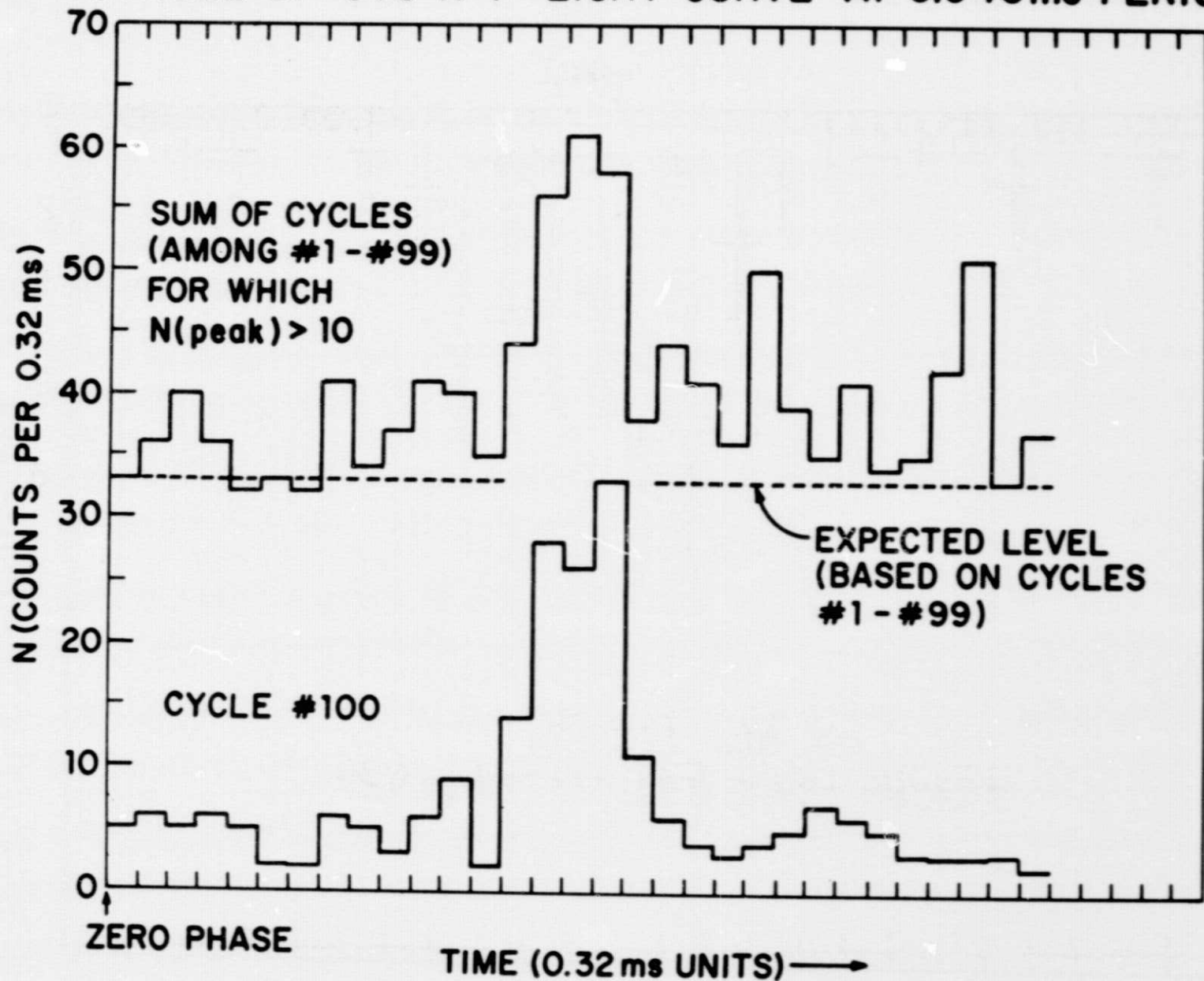


Figure 4

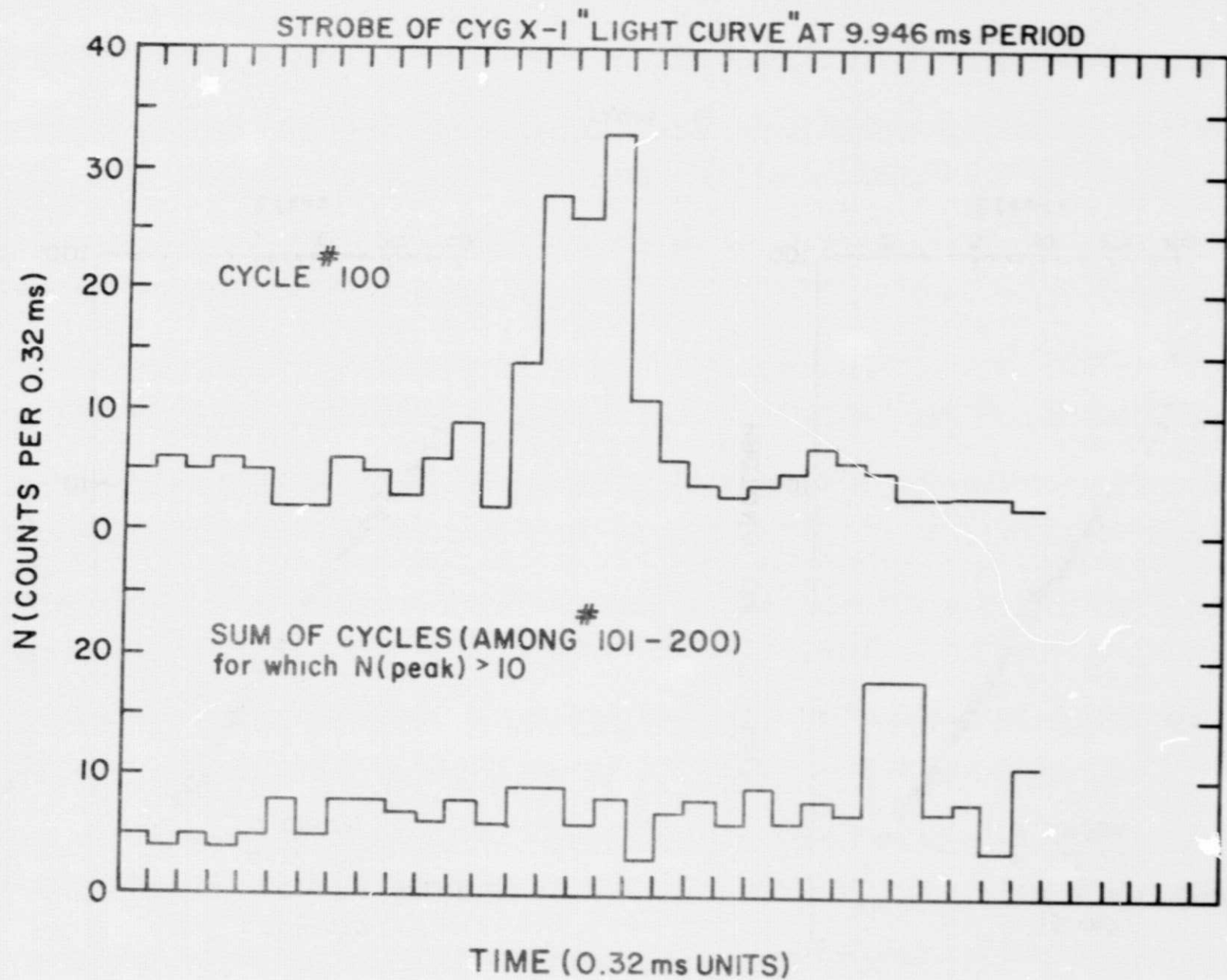


Figure 5

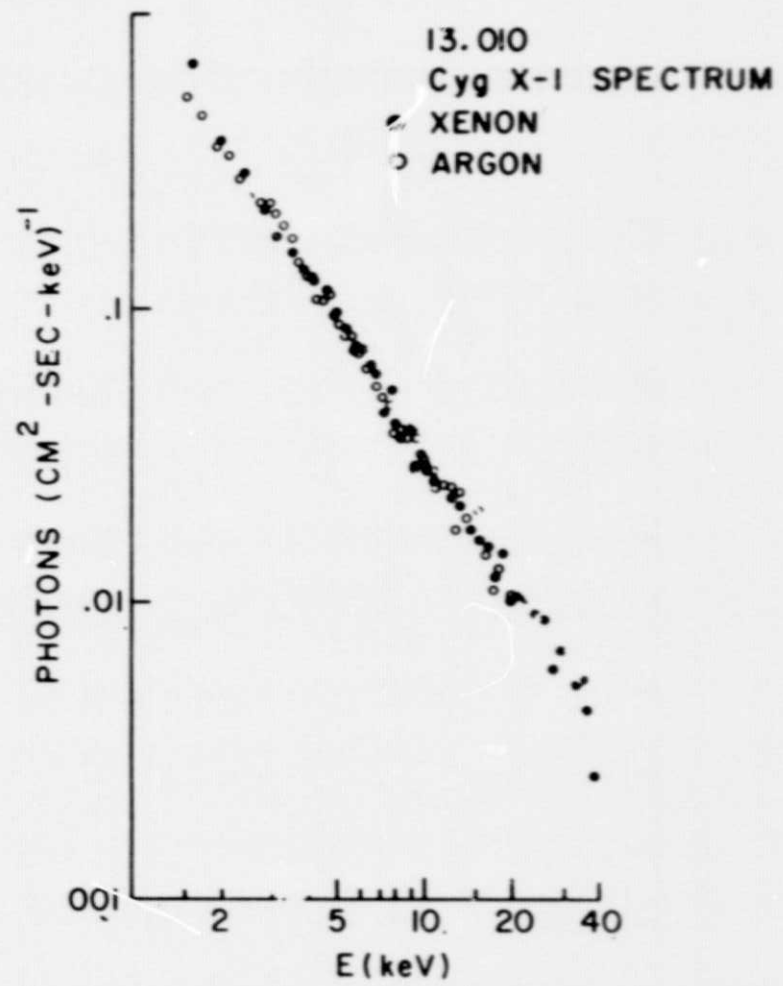
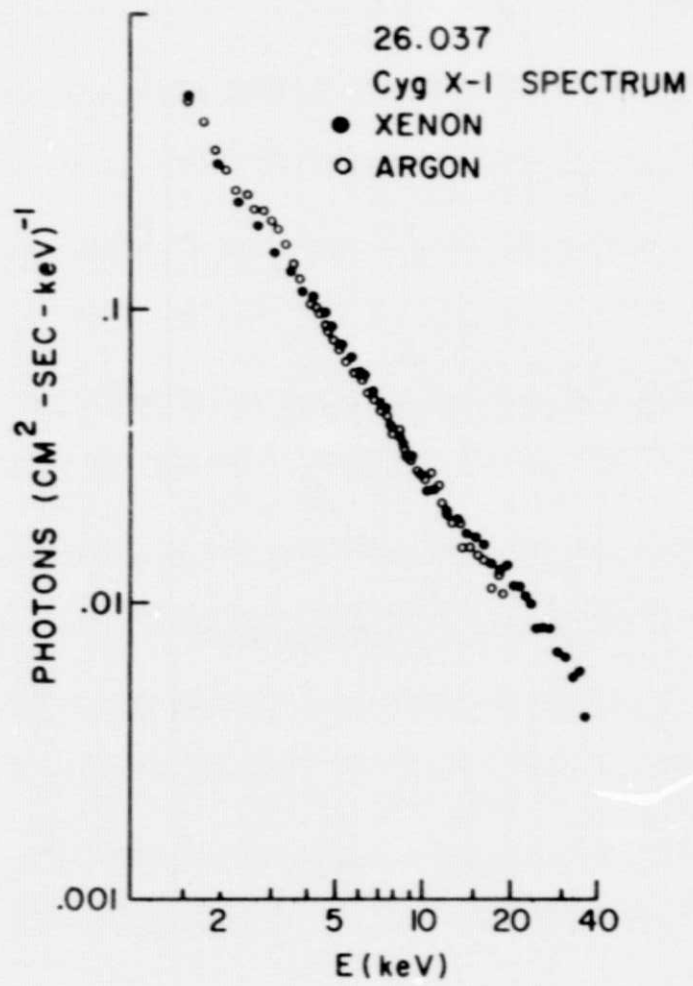


Figure 6

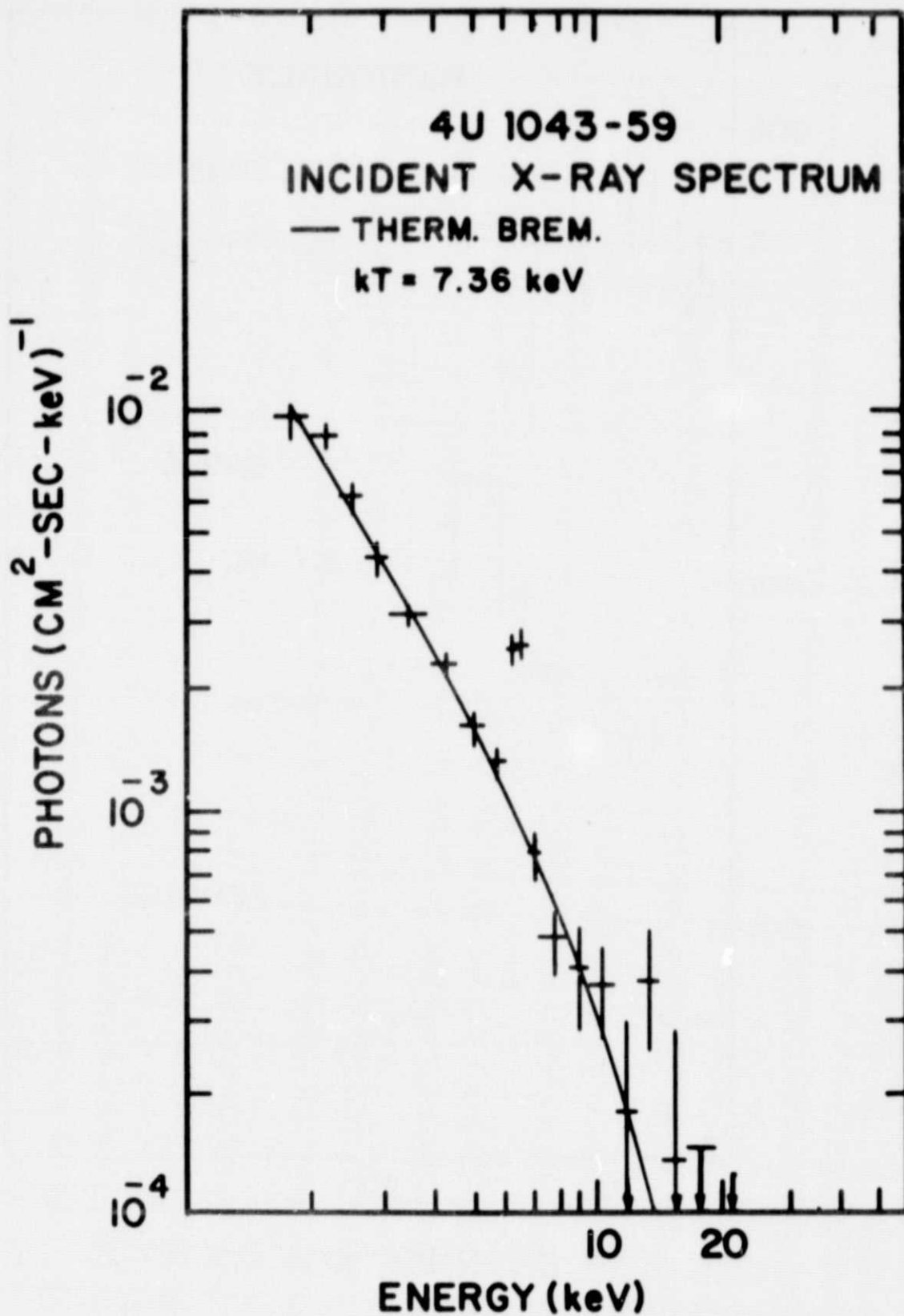


Figure 7

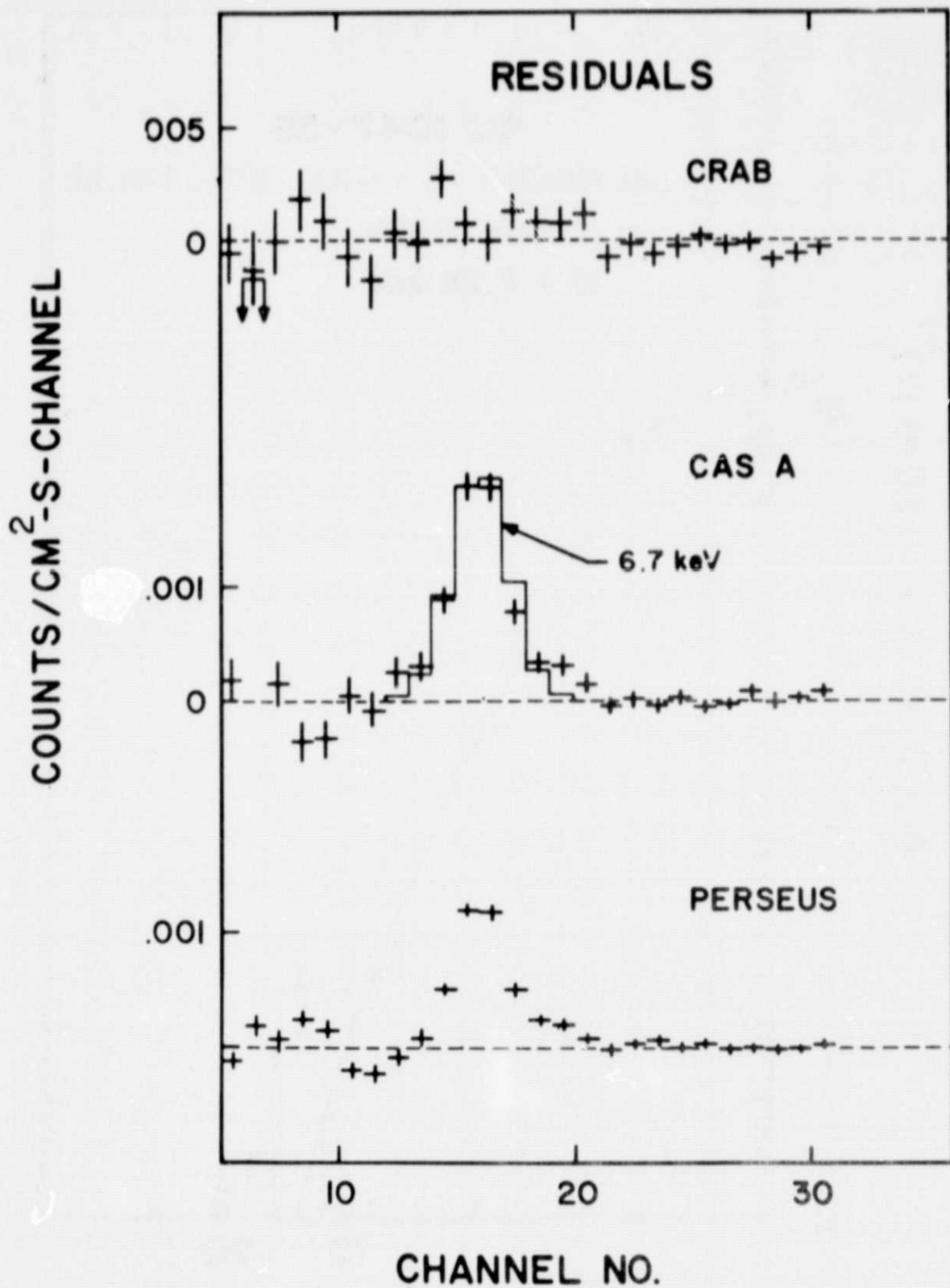


Figure 8

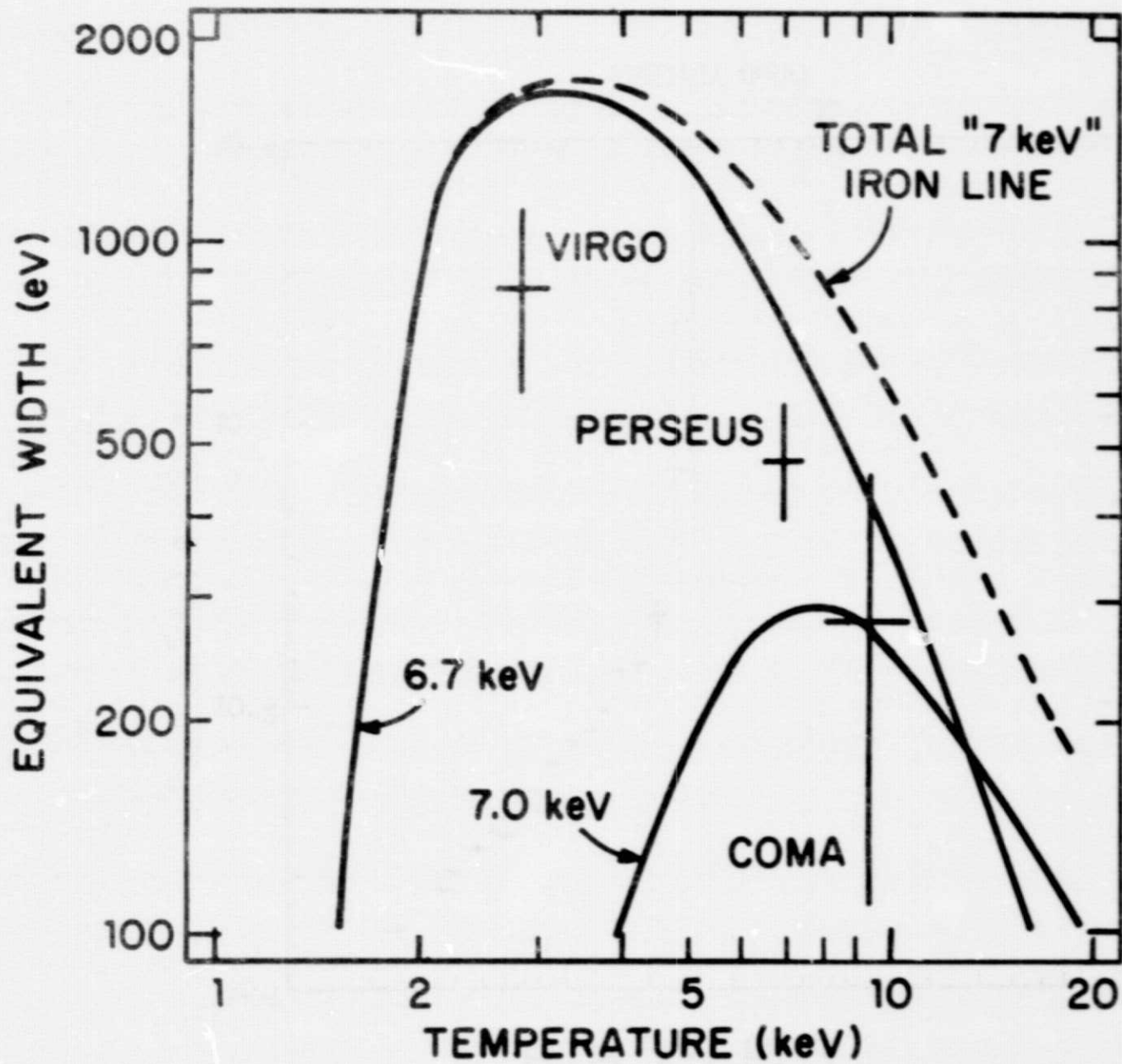


Figure 9

HER X-1 RL2

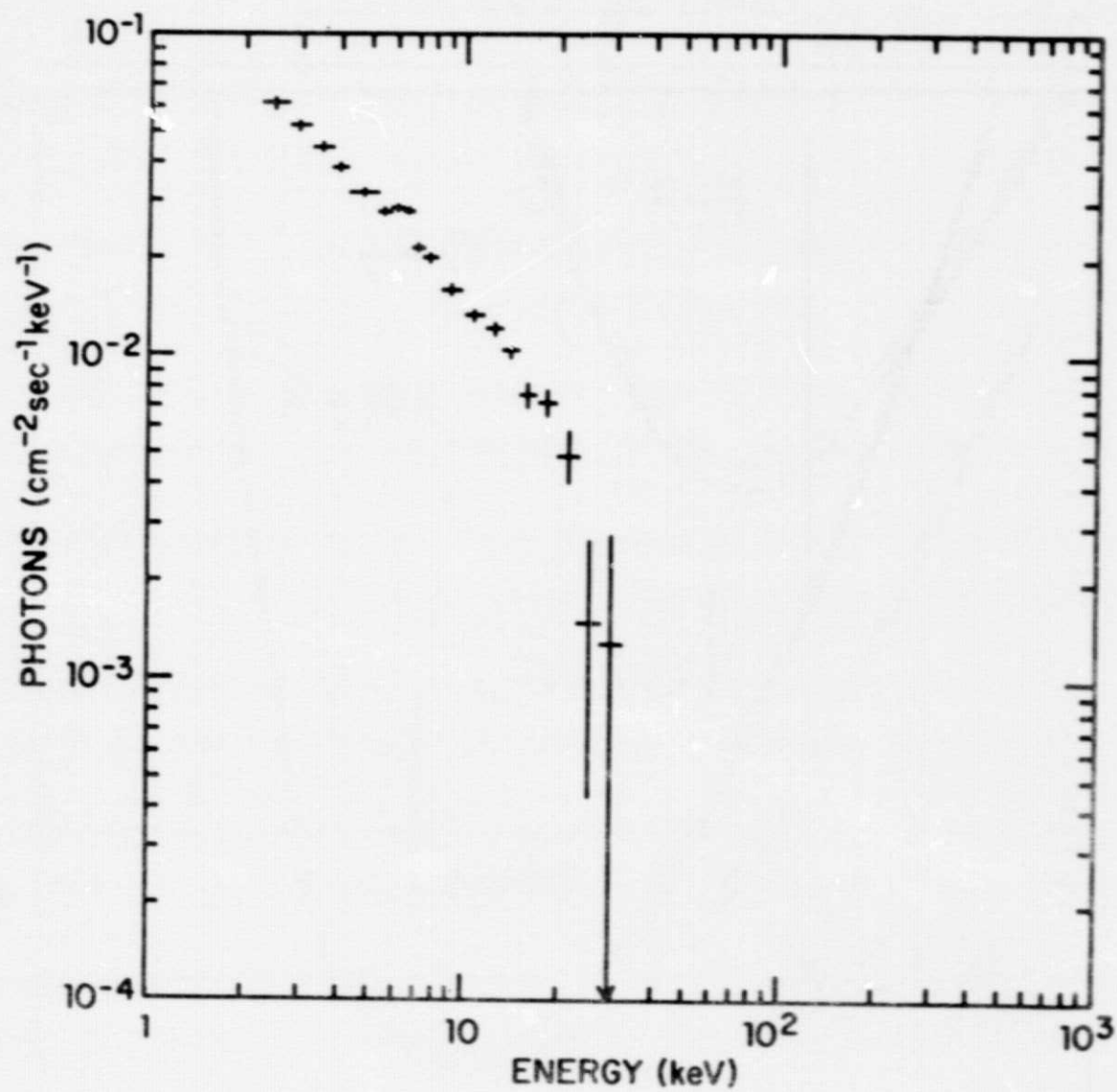


Figure 10

HER X-1 RN1

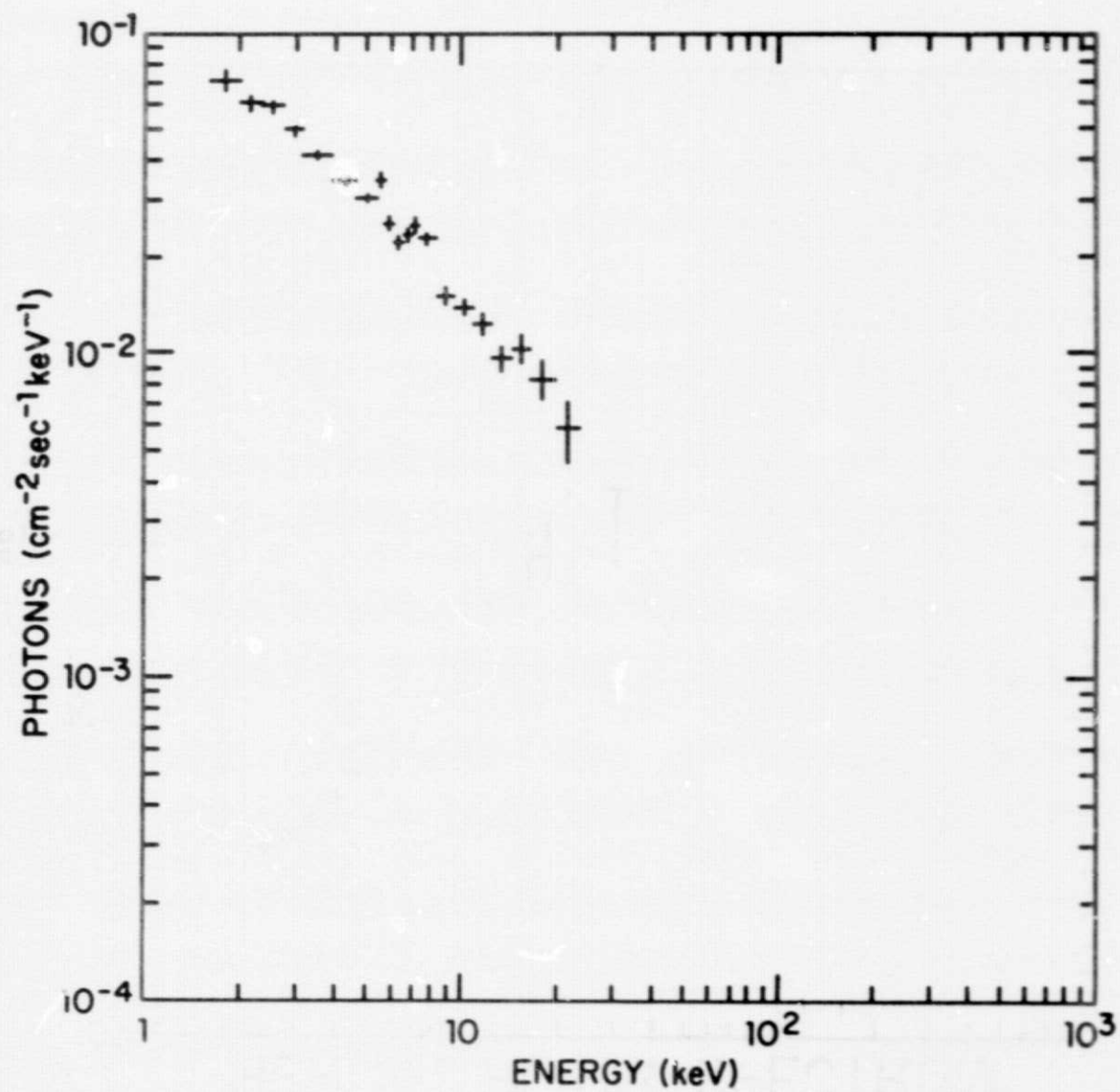


Figure 11

HER X-1 RL:PM SPECTRUM

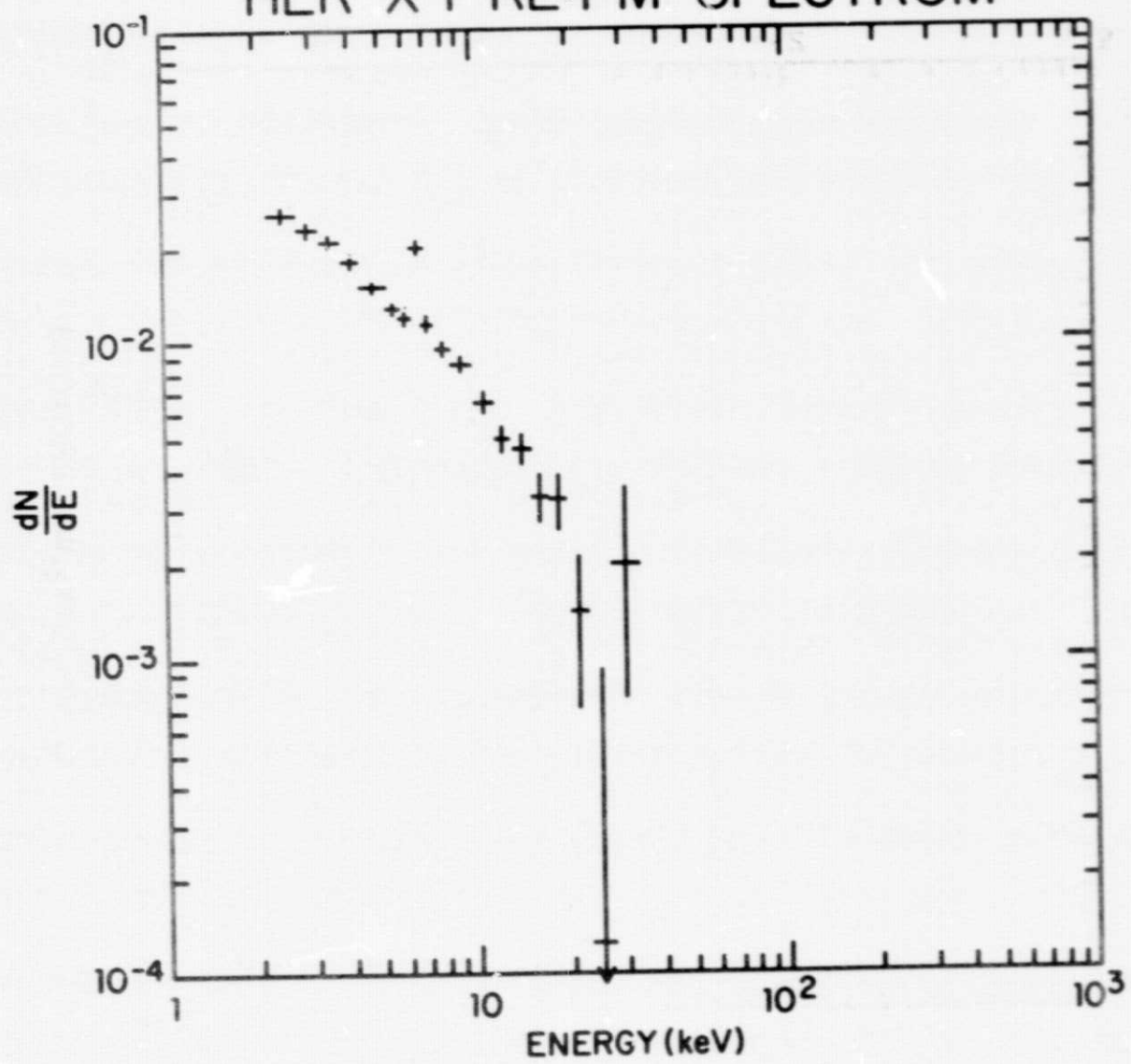


Figure 12